Caliphate Journal of Science & Technology (CaJoST)

ISSN: 2705-313X (**PRINT**); 2705-3121 (**ONLINE**) **Research Article**

Open Access Journal available at: https://cajost.com.ng/index.php/files and https://www.ajol.info/index.php/cajost/index

DOI: https://dx.doi.org/10.4314/cajost.v6i3.10

Article Info

Received: 4th July 2024

Revised: 7th October 2024

Accepted: 11th October 2024

Green Synthesis and Characterization of Iron and Zinc Nano Particles Using Grape Extract

Hauwau S. Lere[1], Gideon Wyasu[1], and Stephen E. Abechi[2]

[1]Department of Pure and Applied Chemistry, Faculty of Physical Science, Kaduna State University Nigeria.
[2]Department of Chemistry, Ahmadu Bello University Zaria, Nigeria.

***Corresponding author's email:**
hauwaulere@gmail.com

Cite this: *CaJoST,* 2024, 3, 333-341

This study focused on the synthesis and characterization of Iron and Zinc nanoparticles using grape extract.. The nanoparticles were characterized using UV-VIS, FTIR, SEM-EDX and XRD spectroscopies. The UV-VIS spectroscopy of iron indicates that the iron nano particle absorb light at 770nm while the zinc nano particle absorb light at 380nm. The utilization of ATR-FTIR spectroscopy of iron revealed distinctive peaks at 3287 cm^{-1}, 2926 cm^{-1}, 1889 cm^{-1}, 1945cm^{-1}, 2012 cm^{-1} to 2072 cm^{-1}, 1919 cm^{-1} and 1817 cm^{-1}, 1379 cm^{-1} and 1038 cm^{-1}, 700 cm^{-1} corresponding to phenol, alkane, A hydride, A hydride, alkyle amine and Fe-bond functional groups respectively. These groups were identified as being responsible for the capping and stabilization of the nanoparticles. That of Zinc revealed distinctive peaks at 3276 cm^{-1} 2922 cm^{-1}, 2113 cm^{-1}, 1636 cm^{-1}, 1543 cm^{-1}, 14011 cm^{-1}, 237 cm^{-1}, and 1028 cm^{-1}corresponding to phenol, alkane, alkyne, alkene, aromatic compound alkene, inorganic carbonate, amine and alkyl amine respectively. Furthermore, EDX analysis confirmed the presence of iron with atomic and weight concentrations of (51.93 and 68.99), and zinc at (20.58 and 35.65) respectively. Scanning Electron Microscope (SEM) micrographs illustrated a uniform distribution and agglomeration of the synthesized iron nano particle (FeNPs) and zinc nano particle (ZnNPs), portraying a near-flat and plain shape with an average particle size of 100 nm. The XRD result revelled that the synthesized iron nano particle (FeNPs) has a crystalline structure with grain size of 23.5nm, while the synthesized zinc nano particle (ZnNP) has a hexagonal structure with grain size of 21.3nm.

Keywords: Grape extract, Zinc nanoparticle, Iron nanoparticle.

1. Introduction

Nanotechnology can be defined as the manipulation of matter through certain chemical and physical processes to create materials with specific properties, which can be used in a particular application. A nanoparticle can be defined as a microscopic particle that has at least one dimension less than 100 nanometres in size (Auffan *et.al.,* 2009). NPs industries are developing metals and metal oxides for the improvement of their services and products. There has been a tremendous increase in nanotechnology in the past decade due to it application in medicine, chemistry, biotechnology and agriculture (Singh *et.al.,* 2008, Whiteside 2005, Pelaz *et.al.,* 2012). These nanoparticles are synthesized using physical, chemical and biological methods. Various physical and chemical methods like hydrothermal, sol-gel synthesis, laser ablation, lithography, etc., require special equipment's and skilled labour. Moreover, they have toxic effects that are hazardous to health. The nanoparticles obtained via green synthesis method are found to be cost-effective, non-toxic, and biodegradable in nature (Virkutyte and Varma 2011, Nadagouda and Varma 2008, Darroudi et.al., 2014, Iravani 2011). This eco-friendly synthesis reduces the use of hazardous substances as the process utilizes the use of fruits, roots, leaves, flower extract and microorganisms like bacteria, fungi, algae etc. (Iravani 2011, Behravan *et.al.,* 2019, Rajiv *et.al.,* 2013, Navale *et.al.,* 2015)

Different research works have shown how different plant extract have been used in the synthesis of iron and zinc nanoparticles such as the use of Andean blueberry extract in the synthesis of iron and zinc (Murguitio *et.al.,* 2022). The use of carica papaya leaf extract (Shakhawat *et.al.,* 2020), Iraqi grape extract (Wisam *et.al.,* 2020), hibiscus rosa extract (Ibrahim *et.al.,* 2024), Artocarpus heterophyllus peel extract (Reena *et.al.,* 2021) and Mulberry fruit extract (Nedra *et.al.,* 2022) in the synthesis of iron and zinc nanoparticles since they do not contain any hazardous chemicals and functions as a natural stabilizing, reducing and caping agent. Many plants sand their parts have evolved in into a superior platform from the production of nanoparticles. (Behravan *et.al.,* 2019).

This research focused on the Green Synthesis of iron and zinc nanoparticles using grape extract, characterization by FTIR for functional groups, SEM for morphology, EDX for elements present with respect to atomic concentration and weight concentration, UV-VIS for atomic spectrum versus, XRD for crystalline structure and sizes

2. Materials and Methods

2.1 Method of extraction of grape juice

The grape extraction was prepared using the methodology outlined by Murgueitio *et al*. (2022), with slight modification (where grape juice was replaced by dried papaya leaf extract) made for optimization. The selection of fruits was based on their specific stage of maturity, and exclusively those exhibiting a deep black color were utilized. A thorough cleaning was implemented on the chosen fruits. Subsequently, both the fruits and stems were meticulously pounded in a mortar to extract the liquid juice. The obtained juice was sieved to eliminate any residual impurities, after which it was carefully transferred onto a filter paper to obtain the refined liquid extract.

2.2 Synthesis of Iron Nanoparticle

50 mL of grape extract was introduced into a 50 mL solution of 0.1 M $FeCl_3.6H_2O$, maintaining a precise 1:1 ratio, which result in the generation of a visually striking black-colored solution. The ensuing mixture underwent a heating process for a duration of 30 minutes, employing a magnetic stirrer. Subsequently, 1 M NaOH was added in droplet to adjust the pH to 11. The mixture turs deep black which indicated the successful formation of iron oxide nanoparticles.

The nanoparticle underwent separation process through centrifugation, operating at 4000rmp for a duration of 30 minutes. The isolated nanoparticles were subjected to a thorough drying process in an oven set at 80^{o}C, for a duration of three (3) hours. The nanoparticle was then stored in an airtight container for characterization (Bibi *et al*. 2019).

2.3 Synthesis of Zinc Nanoparticle

30 mL of grape extract was introduced into 70 mL of a 0.1 M zinc oxide solution which result in the formation of a distinctive brown solution. Subsequently, the solution underwent a 30-minute heating process utilizing a magnetic stirrer 1 M NaOH was added in droplets to adjust the pH to 11. The solution turned dark brown after heating which indicate the successful formation of zinc oxide nanoparticles. The ensuing nanoparticle solution underwent separation by centrifugation at 4000 rpm for a duration of 30 minutes. The isolated nanoparticles were subjected to a final drying process in an oven set at 80°C for a period of 3 hours. The nanoparticles were then stored in an air-tight container for characterization (Bibi *et al.* 2019).

2.4 Characterization of synthesized nanoparticles

2.4.1 Functional Group Analysis

FTIR spectra for both iron and zinc samples were meticulously captured using a cutting-edge FTIR Aligient Technology Cary630FTIR within the wavelength spectrum of 4000-650 cm^{-1}. (Murgueitio *et al.,* 2022).

2.4.2 Absorption Analysis of the Synthesized Nanoparticles

The UV-VIS transmission of both iron and zinc was diagnosed using CARY300 model between the range of 800 to 300nm. 800 to 300 nm. (Murgueitio *et al.,* 2022).

2.4.3 Scanning Electron Microscope (SEM) Analysis and Energy Dispersive X-ray (EDX) Analysis

The scanning electron micrograph (SEM) and EDX analysis of both iron and zinc was done using Phenom Prox (Goldstein *et.al.,2000*, Nathan 2023)

2.4.4 X-Ray Diffraction (XRD) Analysis

X-ray diffraction of both iron and zinc was carried out using (Rigaku Miniflex 600-C) to provide the X-ray patters with a 2Ɵ, scanning angle (2^o-70^o Braggs angle), x-ray tube (Cu abode), operating condition current applied 15Ma and voltage was 40kv. The crystalline size was calculated using Scherrer's equation D = K^/βCos Ɵ (Wisam *et.al.,2020*)

3. Results and Discussion

3.1 ATR-FTIR analysis of synthesize sFeNPs and ZnNPs

The FT-IR spectra analysis of Figure 1A depicting FeNPs reveals a myriad of vibrational peaks associated with biomolecules within the range of 600-4000 cm^{-1}. These peaks play a pivotal role as capping and reducing agents in the formation of FeNPs. They shed light on the functional groups responsible for iron reduction and stabilization. Notably, characteristic peaks at 3287 cm^{-1} and 2926 cm-1 are ascribed to single bond of oxygen and hydrogen (O-H) stretching and carbon-hydrogen (C-H) stretching (Yilleng *et al.,* 2020, Felix *et al.,* 2021), peak observed at 1889 and 1945 are attributed to carbon double bond oxygen (C=O) stretching vibration (Yilleng *et al.,* 2020), 2012 cm^{-1} to 2072 cm^{-1} are attributed to C≡N (Yilleng *et al.,* 2020), 1919 $cm^{-1}$and 1817 cm^{-1} are attributed carbon-carbon-carbon(C=C=C) and carbon doble bond oxygen

(C=O) stretching (Felix *et al.,* 2021),1379 cm^{-1} and 1038 cm^{-1} are attributed to(C-O) stretching and alkyl amine (Nagar and Devra 2018), 700 cm^{-1} ensure the present of Fe-O bond(Bhuiyan *et.al.,*2020 , Aisida et.al2019). These findings elucidate the diverse molecular interactions and bonds involved in the reduction and stabilization of iron, enhancing our understanding of the intricate processes underlying FeNP formation

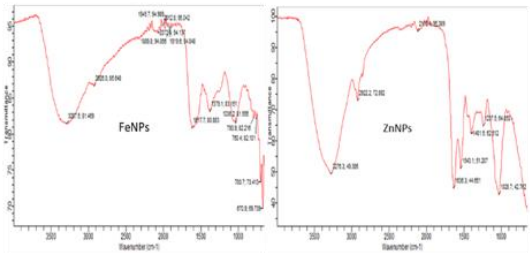

Figure 1.A and 1.B ATR- Fourier transform infrared spectroscopy of zinc nano particle (ZnNPs) and iron nano particle (FeNPs)

The Fourier Transform Infrared (FTIR) analysis, spanning the range of 600-4000 cm^{-1}, not only affirmed the successful synthesis of ZnNPs but also provided insights into the diverse functional groups of reducing agents present in the grape plant fruit extract (refer to Figure 1B). Noteworthy peaks at 3276 cm^{-1} and 2922 cm^{-1} are attributed to the single bonds of oxygen-hydrogen (O-H) stretching and carbon-hydrogen (C-H) stretching, respectively, in alignment with (Aisida *et al.,* 2019). A distinct peak at 2113 cm^{-1} and 1636 are attributed to triple bond of carbon oxygen (C≡O) stretching vibration and carbon carbon (C-C) (Aisida *et al.,* 2019), 1543 cm^{-1} and 1401 cm^{-1} are attributed C-C and -C=O, peak observed at 1237 cm^{-1} is attributed to (C-N) stretching of amine (Kero *et al.,* 2017) and 1028 cm^{-1} for (C-O), aligning with the findings of (Bhuiyan *et al.,* 2020, Aisida *et al.,* 2019). The discernible shifts in peak positions, ranging from 600–4000 cm^{-1}, provide evidence that compounds containing these functional groups are bound to the zinc oxide surface.

The fictional groups found play a crucial role in the synthesis, stabilizing of FeNPs and ZnNPs. Hydroxyl (O-H) and carboxyl (C=O) groups are responsible for capping and reducing agents, stabilizing nanoparticle formation. Alkyl amine (C-N) and carbon-carbon (C-C) groups contribute to nanoparticle stability and biocompatibility. Fe-O and Zn-O bonds indicate nanoparticle formation and iron/zinc oxide presence. Carbon-hydrogen (C-H) and carbon-nitrogen (C≡N) groups contribute to nanoparticle chemistry and potential bioactivity (Bhuiyan *et al.,* 2020, Aisida *et al.,* 2019).

From the result obtained for both iron and zinc the following functional groups are attributed to the plant extract, Hydroxyl (O-H) groups: polyphenols, flavonoid, and other plant derived compounds. Carbon-hydrogen (C-H) groups; plant derived organic compounds such as sugars and amine acids. Carboxyl (C=O) groups; organic acids, flavonoids, and phenolic compounds. Alkyl amine (C-N) groups; amino acids, and protein present in the plant extract (Aisida *et al.,* 2019).

3.2 Ultraviolet-Visible Spectroscopy analysis of FeNPs and ZnNPs

UV-VIS spectroscopy is a commom technique used to analyze the concentration of a substance in a sample based on its absorbance of ultraviolet or visible light. In this case the FeNPs from Figure 2A absorbs light at the wavelength of 770nm which is relatively high suggesting a significant concentration of iron Nano particles in the sample. Higher absorbance value usually corresponds to higher concentration of analyte in the sample. The absorption peak could be related to the size, shape or composition of iron Nano particles. (sorna premarajendra and kandasamy sengodan *2017)*

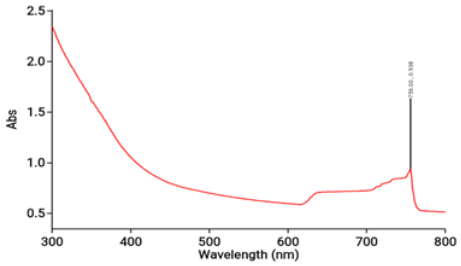

Figure 2.A-UV-VIS spectroscopy of iron nano particle (FeNPs)

From Figure 2B the absorbance value (Abs) indicates the extent to which the ZnNPs absorbs light at 380nm. Absorbance value can range from 0 (no absorption) to higher values with large values indicating strong absorption of light. The wavelength 380nm falls in the UV-visible range of the electromagnetic spectrum. This wavelength is in the visible light region which is typically associated with the absorption of light by materials that have electron transition within this range. The specific wavelength of 380nm could be indicative of certain electronic transitions or energy levels within the zinc Nano particles molecular or atomic structure. The absorption of light at this wavelength may be related to the presence of zinc (Zn) ions or nanoparticles. This result is in line with the actual band gap wave

length of zinc oxide reported by (Sorna premarajandra and kandasamy sengodan *2017*)

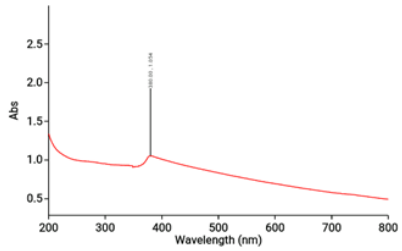

Figure 2.B-UV-VIS spectroscopy of zinc nano particle (ZnNPs)

3.3 Scanning electron microscope (SEM) micrographs and EDX analysis of synthesized of FeNPs and ZnNPs

The Scanning Electron Microscope (SEM) micrographs results of the synthesized FeNF and ZnNPs are presented in Table 1 and 2, along with Figures 3A and 3B. These images collectively convey that the synthesized nanoparticles exhibit a nearly flat and plain shape, characterized by an average particle size of 100 nm. Figure 3A displays a distinctive uniform distribution of nanoparticles, accompanied by noticeable agglomeration, possibly attributed to the concentration of the precursor employed.

Grape extracts were utilized for the biosynthesis of Fe nanoparticles, intended for applications inantibacterial, antioxidant, and cytotoxicity domains. The particle size reported in this study surpasses that documented by (Ilham *et al., 2022*) and (Alankrita *et al. 2022*) while being inferior to the findings of (Shweta *et al., 2022*). This variance could stem from disparities in the choice of precursors or the specific reaction conditions employed.

Furthermore, the SEM micrographs for ZnNPs from figure 3B reveal a non-uniform distribution and agglomeration of nanoparticles, likely influenced by the concentration of the precursor used grape extract (Ilham *et.al., 2022)*

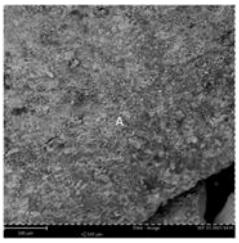

Plate 1.A-SEM, B-EDX micrograph of iron nano particle (FeNPs)

Table 1. EDX analysis of iron nano particle (FeNPs)

Element Number	Element Symbol	Element Name	Atomic Conc.	Weight Conc.
26	Fe	Iron	51.93	68.99
11	Na	Sodium	20.26	11.08
14	Si	Silicon	8.08	5.40
17	Cl	Chlorine	5.23	4.41
13	Al	Alluminium	5.40	3.47
12	Mg	Magnesium	3.79	2.19
15	P	Phosphorus	1.97	1.45
16	S	Sulfur	1.30	1.00
19	K	Potassium	1.03	0.96
20	Ca	Calcium	0.71	0.67
25	Mn	Manganese	0.29	0.38
22	Ti	Titanium	0.00	0.00

Energy dispersive X-ray (EDX) analysis was employed to elucidate the elemental composition of the synthesized nanoparticles. As depicted in plate 3 and 4, and detailed in Tables 1 and 2, the analysis revealed the prominent presence of iron (Fe) with atomic concentration and weight concentration of (51.93,68.99), Na (20.26,22.08), Si (8.08,5.40), Cl (5.23,4.41), Al (5.40,3.47), Mg (3.79,2.19), P (1.97,1.45), S (1.30,1.00), K (1.03,0.96), Ca (0.71,0.67) Mn (0.29,0.38), Ti (0.00,0.00)

From table 2 result of EDX for ZnNPs revealed Zn with the highest atomic concentration and weight concentration of (20.58,35.65), Ca (32.93,34.97), Na (36.46,22.22), Mg (4.97,3.20), Al (1.94,1.38), Si (1.41,1.05), P (0.81,0.66), S (0.43,0.36), Cl (0.21,0.20), K (0.16,0.17), Ti (0.11,0.13), Fe (0.00,0.00). where iron did not show any noticeable indication. The result obtained was similar to that of (Judith et.al.,2021and Sheoran et.al.,2021).

The presence of sodium (Na) and calcium (Ca) can be as a result of impurities or from the grape extract. Potassium (K) is present from the precursor grape extract. Silicon (Si), Alluminium (Al) and Titanium (Ti) presence may be due to impurities from equipment or containers or environmental contamination. Chlorine (Cl), Sulfur (S) and Phosphorus presence may be residual component from plant extract or impurities from starting materials (Sheoran et.al.,2021).

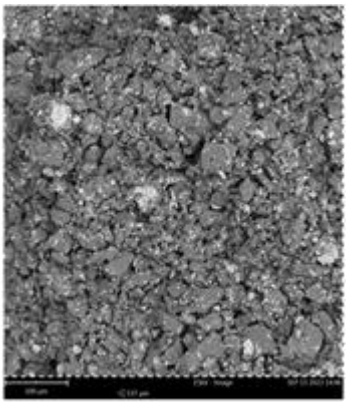

Plate 1.B-SEM, B-EDX micrograph of zinc nano particle (ZnNPs)

Table 2. EDX analysis of zinc nano particle (ZnNPs)

Element Number	Element Symbol	Element Name	Atomic Conc.	Weight Conc.
30	Zn	Zinc	20.58	35.65
12	Mg	Magnesium	4.97	3.20
13	Al	Aluminium	1.94	1.38
14	Si	Silicon	1.41	1.05
15	P	Phosphorus	0.81	0.66
16	S	Sulfur	0.43	0.36
17	Cl	Chlorine	0.21	0.20
19	K	Potassium	0.16	0.17
22	Ti	Titanium	0.11	0.13
26	Fe	Iron	0.00	0.00

3.4 X-ray Diffraction (XRD) analysis of synthesized FaNPs and ZnNPs

Plate 4A shows the XRD result of iron nano particle (FeNP) at 2ϴdegree = 28.5º which matches the (012) plane of Hematite (Fe_3O_3) corresponding to the international center for diffraction data (ICCD) card number 00-001-1053. The result shows that the synthesized FeNP have a crystalline structure consistent with Hematite indicating a trigonal system (Kiwumulo *et.al,* 2022). The crystalline grain size of the FeNP was calculated and found to be 23.5nm (Kumar and Prem 2018). Research have highlighted the potential of green synthesis methods such as using grape for production of Fe nano particles. These methods offer environmental benefits and produce nano particles with control size and shape. (Fang *et.al,.*2014). The unclarity of peaks may be due to crystalline impurities because present of impurities obscures peaks, or resolution, scanning rate or beam quality issues can also affect peak clarity (Kiwumulo *et.al,* 2022). The noise may be a result of background radiation, instrumental noise or sample related noise (e.g., surface roughness) (Kiwumulo *et.al,* 2022). Therefore, the peaks were identified using international center for diffraction database.

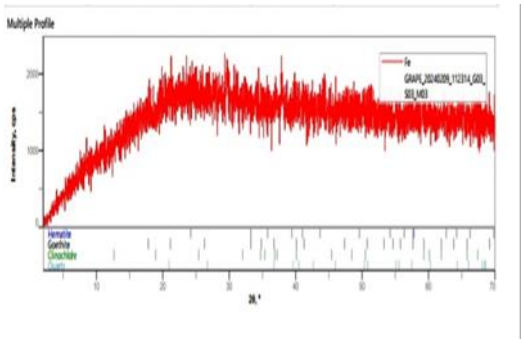

Plate 2.A- XRD analysis of iron nano particle (FeNPs)

Plate 4B shows the result of zinc nano particle (ZnNP) indicating diffraction peak at 2ϴdegrre =26.66º,29.452º, 31.07º, 34.44º, 36.33º, 47.639º, 48.67º, 56.61º, 62.827º, and 69.052º corresponding to the lattice plane of (101) (104) (104) (100) (102) (101) (102) (116) (110) (103) (112) and (201) respectively (Jayachandra *etal,2022* , Shah *et.al.,2021).* The peaks were matched with the international center for diffraction data (ICCD) card number 04-013-6607. The synthesized zinc nano particle (ZnNP) has a hexagonal structure (Ashwini *et.al.,2021*). The crystalline size was calculated and founded to be 21.3nm (Shah *et.al.,2021.*, Ashwini *et.al.,2021*)

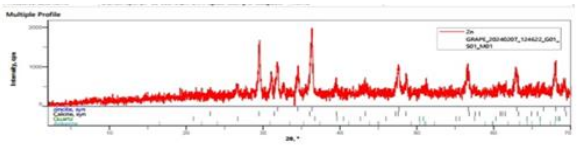

Plate 2.B-XRD analysis of zinc nano particle (ZnNPs)

4. Conclusion

In conclusion, the successful synthesis of iron, zinc nanoparticles were achieved through the utilization of grapefruit extract as both a stabilizing and capping agent. The UV-VIS of FeNP shows that it absorbed light at maximum peak of 770nm and ZnNP absorbed light at maximum peak of 380nm. The ATR-FTIR analysis of FeNP unveiled distinctive peaks at 3287 cm^{-1}, 2926 cm^{-1}, 1889cm^{-1}, 1945 cm^{-1} to 1919 cm^{-1}, and 1817cm^{-1}, 1379 cm^{-1} and 1038 cm^{-1} corresponding to alkyl halides, aldehydic, aromatic, amines, amine, and carboxylic acid functional groups, that of ZnNP is 3276, 2922,2113,1237,1028 which also correspond to These groups played crucial roles in the capping and stabilizing processes of the nanoparticles. The XRD result revelled that FeNP is trigonal in

shape with grain size of 23.5nm while ZnNP is hexagonal with grain size of 21.3nm. Furthermore, EDX analysis exhibited the presence of iron with atomic and weight concentrations of (51.93 and 68.99), and zinc with concentrations of 20.58 and 35.65, respectively. Scanning Electron Microscope (SEM) micrographs of the synthesized FeNPs and ZnNPs demonstrated a homogeneous distribution and agglomeration of the nanoparticles. The morphology appeared nearly flat and plain, with an average particle size of 100 nm. Interestingly, the iron nanoparticles displayed superior features compared to zinc counterparts base on its characterization.

Conflict of interest

The authors declare no conflict of interest.

Acknowledgements

The authors would like to acknowledge Multipurpose Research Laboratory of Chemistry department Ahmadu Bello University Zaria for allowing me access the characterization equipment for the Characterization and National Steel Raw Material Exploration Agency (NSRMEA) Malali Kaduna.

References

Aisida S.O., Madubuonu N., Alnasir M.H., Ahmad I., Botha S., Maaza M., Ezema F.I. (2019). Biogenic synthesis of iron oxide nanorods using Moringa oleifera leaf extract for antibacterial applications. Applied Nanoscience. 10, 305–315

Alankrita, D., Kavita, R., Shani, R., Kanika, S. (2022) Synthesis of silver nanoparticles employing *Polyalthia longifolia* leaf extract and there *in vitro* antifungal activity against phytopathogen. Biochemistry and Biophysics Reports. 31 101320. https://doi.org/10.1016/j.bbrep.2022.101320.

Ashwini, J.; Aswathy, T. R.; Rahul, A. B.; Thara, G. M.; Nair, A. S. (2021). Synthesis and Characterization of Zinc Oxide Nanoparticles Using Acacia caesia Bark Extract and Its Photocatalytic and Antimicrobial Activities. *Catalysts 2021*, 11, 1507

Askary, M., Amirjani, M. R., and Saberi, T. (2017). Comparison of the effects of nano-iron fertilizer with iron-chelate on growth parameters and some biochemical properties of Catharanthus roseus. J. Plant Nutr., 40, pp. 974–982.

Bhuiyan Md.S.H., Miah M.Y., Paul S.C., Aka T.D., Saha O., Rahaman Md.M., Md. Sharif J.I., Habiba O., and Ashaduzzaman Md. (2020). Green synthesis of iron oxide nanoparticle using Carica papaya leaf extract: application for photocatalytic degradation of remazol yellow RR dye and antibacterial activity. Heliyon 6, e04603.

B. Pelaz, S. Jaber, D.J. De Aberasturi, V. Wulf, T. Aida, J.M. de la Fuente, N. A. Kotov (2012)
The state of nanoparticle-based nanoscience and biotechnology: progress, promises, and challenges, ACS Nano 6 (2012) 8468–8483, https://doi.org/ 10.1021/nn303929a.

Bibi, I., Nazar, N., Ata, S., Sultan, M., Ali, A., Abbas, A., Jilani, K., Kamal, S., Sarim, F.M.,Khan, M.I., Jalal, F., Iqbal, M. (2019). Green synthesis of iron oxide nanoparticlesusing pomegranate seeds extract and photocatalytic activity evaluation for thedegradation of textile dye. J Mater Res Technol 8 (6), pp. 6115–6124.

Chin-Chun Chung and Jiunn-Jer Hwang. (2022). Porous Diatomaceous Earth/Nano-Zinc Oxide Composites: Preparation and Antimicrobial Applications, J. Compos. Sci. 7(5), 204; https://doi.org/10.3390/jcs7050204

Dalal Ibrahim, Karema Abdelghani, Safa Anwagy, Rowedah Rizkallah (2024)
Synthesize Iron Oxide and Zinc Oxide Nanoparticles Using Plant ExtractsDepartment ofChemistry,Faculty of Science, Omar Al-Mukhtar University, Albyda, Libya © 2024 by the authors. Submitted for possible open access publication under the terms and conditions of the Creative Commons Attribution International License (CC BY 4.0). http://creativecommons.org/licenses/by/4.0

Fang, Lusheng et al. (2015). Endocytosis and its regulation in plants. Trends in Plant Science, [s. l.], v. 20, n. 6, p. 388–397

Felix, Z., Adrián, L., Fernando, O., Gloria, Q., Carmen, G., Gemma, M. (2021). Introducing ATR-FTIR Spectroscopy through Analysis of Acetaminophen Drugs: Practical Lessons for Interdisciplinary and Progressive Learning for Undergraduate Students. Journal Chemistry Education, 98, 2675−2686. https://doi.org/10.1021/acs.jchemed.0c01231 fenvs. 2016. 00020

Generalic, Eni. (2023). Prepartion of Solutions. EniG.Periodic table of the elements.KTF-Split.

G.M. Whitesides, Nanoscience, nanotechnology, and chemistry, Small 1 (2005) 172–179, https://doi.org/10.1002/smll.200400130.

G.R. Navale, M. Thripuranthaka, D.J. Late, S.S. Shinde (2015)
Antimicrobial activity of ZnO nanoparticles against pathogenic bacteria and fungi, JSM Nanotechnol
Nanomed 3 (2015) 1033.

Goldstein, J. I., Newbury, D. E., Echlin, P., Joy, D. C., Fiori, C., Lifshin, E. (2000). Scanning Electron Microscopy and X-ray Microanalysis. Springer Science & Business Media.

Ilham, M., Dhiaulhaq, F., Binawati, G. (2022) Biosynthesis of Cu nanoparticles using *Polyalthia longifolia* roots extracts for antibacterial, antioxidant and cytotoxicity applications. *Materials Technology*. (37), 13, 2517–2521.
https://doi.org/10.1080/10667857.2022.2044217

J. Virkutyte, R.S. Varma (2011)
Green synthesis of metal nanoparticles: biodegradable polymers and enzymes in stabilization and surface functionalization, Chem. Sci. 2 (2011) 837–846, https://doi.org/10.1039/C0SC00338G.
Judith C., Miguel A., Benjamín V., Federico G., Carlos C., Blanca L., Daniel G. (2021) Synthesis and Characterization of Green Potassium Nanoparticles from Sideroxylon Capiri and Evaluation of Their Potential Antimicrobial. *JRM*. DOI: 10.32604/jrm.2021.015645.

Kero Jemal, B. V. Sandeep, and Sudhakar Pola. (2017). Synthesis, Characterization and Evaluation of the Antibacterial Activity of *Allophylus serratus* Leaf and Leaf Derived Callus Extracts Mediated Silver Nanoparticles. Journal of Nanomaterials Volume 2017, Article ID 4213275, 11 pages https://doi.org/10.1155/2017/4213275

Khanm, H., Vaishnavi, B. A., Namratha, M. R. and Shankar, A. G. (2017). Nano zinc oxide boosting growth and yield in Tomato: the rise of “nano fertilizer era”.*Int. J. Agric. Sci. and Res.*, 7(3): 197- 206.

Kumar, R., Ashfaq, M., and Verma, N. (2018). Synthesis of novel PVA-starch formulation-supported Cu-Zn nanoparticle carrying carbon nanofibers as a nanofertilizer: controlled release of micronutrients. J. Mater. Sci. 53, 7150 Sci. 53, 71501007/s10853-018-2107-9

Kumar, V. G. Viju & Prem, Ananthu A. 2018. Green Synthesis and Characterization of Iron Oxide
Nanoparticles Using Phyllanthus Niruri Extract. Oriental Journal of Chemistry 34(5):2583–2589.

Kiwumulo H. F.; Haruna M.; Charles I.; Michael L.; John B. K.; Robert T. S. (2022). Green synthesis and characterization of iron-oxide nanoparticles using *Moringa oleifera*: a potential protocol for use in low

and middle-income countries, *BMC Research Notes*, 15; 149

López-Vargas ER, Ortega-Ortíz H, Cadenas-Pliego G, De Alba Romenus K, Cabrera de la Fuente M, Benavides-Mendoza A, Juárez Maldonado A (2018) Foliar application of copper nanoparticles increases the fruit quality and the content of bioactive compounds in tomatoes. Appl Sci 8:1020

M. Auffan, J. Rose, J.-Y. Bottero, G. V. Lowry, J.-P. Jolivet, and M. R. Wiesner, (2009)
“Towards a definition of inorganic nanoparticles from an environmental, health and safety perspective,”Nature Nanotechnology, vol. 4, pp. 634–641, 2009

M. Singh, S. Singh, S. Prasad, I.S. Gambhir. (2008)
Nanotechnology in medicine and antibacterial effect of silver nanoparticles, Dig. J. Nanomater. Bios. 3 (2008) 115–122.

M. Darroudi, Z. Sabouri, R.K. Oskuee, A.K. Zak, H. Kargar, M.H.N.A. Hamid (2014)
Green chemistry approach for the synthesis of ZnO nanopowders and their cytotoxic effects, Ceram. Int. 40 (2014) 4827–4831, https://doi.org/10.1016/j.
ceramint.2013.09.032.

M. Behravan, A.H. Panahi, A. Naghizadeh, M. Ziaee, R. Mahdavi, A. Mirzapour (2019)
Facile green synthesis of silver nanoparticles using Berberis vulgaris leaf and root aqueous extract and its antibacterial activity, Int. J. Biol. Macromol. 124 (2019) 148–154, https://doi.org/10.1016/j.ijbiomac.2018.11.101.

Md. Shakhawat Hossen Bhuiyan, Muhammed Yusuf Miah, Shujit Chandra Paul,Tutun Das Aka , Otun Saha , Md. Mizanur Rahaman , Md. Jahidul Islam Sharif ,Ommay Habiba, Md. Ashaduzzaman (2020)

Green synthesis of iron oxide nanoparticle using Carica papaya leaf extract:application for photocatalytic degradation of remazol yellow RR dye andantibacterial activity.Department of Applied Chemistry and Chemical Engineering, Noakhali Science and Technology University, Sonapur 3814, https://doi.org/10.1016/j.heliyon.2020.e04603

M.N. Nadagouda, R.S. Varma (2008)
Green synthesis of silver and palladium nanoparticles at room temperature using coffee and tea extract, Green Chem. 10 (2008) 859–862, https://doi.org/10.1039/B804703K.

Murguetio-Herrera, E.; Falconí, C.E.; Cumbal, L.; Gómez, J.;Yanchatipán, K.; Tapia, A.; Martínez,K.; Sinde-Gonzalez, I.; Toulkeridis, T. (2022). Synthesis of Iron, Zinc, andManganese Nanofertilizers, UsingAndean Blueberry Extract, and Their Effect in the Growth of Cabbage andLupin Plants. Nanomaterials, 12, 1921. https://doi.org/10.3390/nano12111921

Nagar N., and Devra V. (2018). Green synthesis and characterization of copper nanoparticles using *Azadirachta indica* leaves, Journal of Materials Chemistry and Physics, doi: 10.1016/ j. matchemphys.2018.04.007.

Nair, K. Madhavan; Augustine. (2018). Little Flower. Food synergies for improving bioavailability of micronutrients from plant foods. Food Chemistry, [s. l.], v. 238, p. 180–185.

Nathan D A. (2023). Green Synthesis OF Eco-friendly Potasium Nanoparticles and its Application on *Amarathus Viridis, Solanum Lycopersocum* and *Hibiscussabdariffa* Plants. Msc. Chemistry, Department of Pure and Applied Chemisty, Faculty of Physical Science, Kaduna State University Kaduna-Nigeria. 1, 40-41.

Nedra ABBES, Imene BEKRI, Meilin CHENG, Nejib SEJRI,Morched CHEIKROUHOU ,Jun XU (2022)
Green Synthesis and Characterization of Zinc Oxide Nanoparticles Using Mulberry Fruit and Their Antioxidant ActivitySchool of Textile Science and Engineering, Tiangong University, Tianjin 300000, China Textile Engineering Laboratory (LGTEX), Monastir University, Monastir 5000, Tunisia National Center of Materials Science, Techno-pole, Borj Cedria, Slimene 2084, Tunisia http://dx.doi.org/10.5755/j02.ms.28314

P. Rajiv, S. Rajeshwari, R. Venkatesh (2013)
Bio-Fabrication of zinc oxide nanoparticles using leaf extract of Parthenium hysterophorus L. and its size-dependent antifungal activity against plant fungal pathogens, Spectrochim. Acta Mol. Biomol. Spectrosc. 112 (2013) 384–387, https://doi.org/10.1016/j.saa.2013.04.072.

Reena Jain a, Swati Mendiratta a, Lalit Kumar b, Anju Srivastava a,
Green synthesis of iron nanoparticles using Artocarpus heterophyllus peelextract and their application as a heterogeneous Fenton-like catalyst for thedegradation of Fuchsin Basic dyeDepartment of Chemistry, Hindu College, University of Delhi, Delhi, 110007, India, Department of Physics, Hindu College, University of Delhi, Delhi, 110007, Indiahttps://doi.org/10.1016/j.crgsc.2021.100086

S. Iravani (20011) Green synthesis of metal nanoparticles using plants, Green Chem. 13 (2011) 2638–2650, https://doi.org/10.1039/C1GC15386B.

Shah, F.; Hasnain, J.; Sajjad, A. S.; Sumaira, Sh.; Adnan, K.; Muhammad, T. A.; Muhammad, R.; Faheem, J.; Wajidullah, N. A.; Aishma, K.; Suliman, S. (2021). Green Synthesis of Zinc Oxide (ZnO) Nanoparticles Using Aqueous Fruit Extracts of Myristica fragrans: Their Characterizations and Biological and Environmental Applications, *ACS Omega 2021*, 6, 9709−9722

Sheoran, P., Goel, S., Boora, R., *et al*. (2021) Biogenic synthesis of potassium nanoparticles and their evaluation as a growth promoter in wheat. *Plant Gene.* Doi.org/10.1016/j.plgene.2021.100310

Shweta B., Vinay S., Nilima K. (2022) Biosynthesized magnetite nanoparticles from *Polyalthia longifolia* leaves improve photosynthetic performance and yield of *Trigonella foenum-graecum* under drought stress. *Plant Stress*. doi.org/10.1016/j.stress.2022.100090.

Sofy, A.R.; Sofy, M.R.; Hmed, A.A.; Dawoud, R.A.; Alnaggar, A.E.A.M.; Soliman, A.M.; Dougdoug, N.K.E. (2021). Ameliarating the Adverse Effects of Tomato mosaic tobamovirus Infecting Tomato Plants in Egypt by Boosting Immunity in Tomato Plants Using Zinc Oxide Nanoparticles. Molecules. 26, pp. 1337.

Sorna Prema Rajendran and Kandasamy Sengodan

Synthesis and Characterization of Zinc Oxide andIron Oxide Nanoparticles Using Sesbania grandiflora LeafExtract as Reducing AgentDepartment of Food Technology, Kongu Engineering College, Perundurai 638 052, IndiaCorrespondence should be addressed to Sorna Prema Rajendran; sornarajendran42@gmail.comReceived 22 June 2016; Accepted 18 December 2016; Published 3 January 2017.

Wisam J. Aziz1, Muslim A. Abid1, Duha A. Kadhim1, Mohanad Kadhim Mejbel2
Synthesis of iron oxide (β-fe2o3) nanoparticles from Iraqi grapes
extract and its biomedical application
1Department of Physics, College of Science, Mustansiriayah University, Baghdad, Iraq.
2Materials Techniques Engineering Department, Engineering Technical College, Baghdad, Middle Technical University (MTU), Iraq. IOP Conf. Series: Materials Science.

Yilleng TM., Samuel NY., Stephen D., Akande JA., Agendeh ZM., and Madaki LA. (2020). Biosynthesis of Copper and Iron Nanoparticles using Neem (*Azadirachta indica*) Leaf Extract and their Anti-bacterial Activity, Journal of applied Science and Environmental Management. Vol. 24 (11) 1987-1991. DOI: https://dx.doi.org/10.4314/jasem.v24i11.20.

